# Supplement to First direct measurements of formaldehyde flux via eddy covariance from a coniferous forest

J. P. DiGangi[1], E. S. Boyle[1], T. Karl[2], P. Harley[2], A. Turnipseed[2], S. Kim[2], C. Cantrell[2], R. L. Maudlin III[2,3,7], W. Zheng[2], F. Flocke[2], S. R. Hall[2], K. Ullmann[2], Y. Nakashima[6], J. B. Paul[4], G. M. Wolfe[1], A. R. Desai[5], Y. Kajii[6], A. Guenther[2], and F. N. Keutsch[1]

[1]Department of Chemistry, University of Wisconsin-Madison, Madison, WI, USA
[2]Atmospheric Chemistry Division, National Center for Atmospheric Research, Boulder, CO, USA
[3]Department of Physics, University of Helsinki, Finland
[4]Thermo Fisher Scientific, Redwood City, CA, USA
[5]Department of Atmospheric & Oceanic Sciences, University of Wisconsin-Madison, Madison, WI, USA
[6]Division of Applied Chemistry, Faculty of Urban Environmental Sciences, Tokyo Metropolitan University, Japan
[7]Now at: Department of Atmospheric and Oceanic Sciences, University of Colorado, Boulder, CO, USA

*Correspondence to:* F. N. Keutsch
(keutsch@chem.wisc.edu)

## S1 HCHO Permeation Tube Calibration

The FTIR gas cell pressure and temperature were held near ambient. Spectra were acquired and integrated for 1 hr at 1 $cm^{-1}$ resolution. The concentration of formaldehyde (HCHO) in the calibration mixture was quantified using HITRAN absorption line lists (Rothman et al., 2005) and a multi-component least squares fitting algorithm (Griffith, 1996). The C-H stretch region of 2620-2920 $cm^{-1}$ was chosen as the fitting region. The permeation rate determined via FTIR spectroscopy was found to be significantly lower ($\sim$50%) than the rate determined via mass loss over time.

## S2 Error in Flux Measurements

Error resulting from instrument response time was estimated by:

$$\frac{\Delta \overline{w'HCHO'}}{\overline{w'HCHO'}_{meas}} = 2\pi f_m \tau_{HCHO} \tag{S1}$$

where $f_m$ is the frequency maximum of the weighted cospectrum (Fig. 3a) and $\tau_{HCHO}$ is the instrument response time, determined from the decay observed upon introducing a sharp concentration change at the front of the inlet (Horst, 1997). The measured instrument response time of $\sim$0.28 s resulted in an estimated error of $\leq$ 5%. Error from instrumental noise as a result of the discrete method of detection (i.e. shot noise) was estimated by the following equation:

$$\frac{\Delta \overline{w'HCHO'}}{\overline{w'HCHO'}_{meas}} = \frac{\sigma_w^2 \sigma_{HCHO}^2}{f_s T} \tag{S2}$$

where $\sigma_x^2$ is the measurement variance in $x$, $f_s$ is the sampling frequency, and $T$ is the length of the sampling period (Lenschow and Kristensen, 1986; Ritter et al., 1990). This typically resulted in an error of $< 4\%$. Error due to the separation between the HCHO inlet and sonic anemometer was determined by the following cospectral transfer function:

$$T_s(f) = e^{-9.9\left(\frac{fs}{U}\right)^{1.5}} \tag{S3}$$

where $f$ is the cospectral frequency, $s$ is the sensor separation, and $U$ is the wind speed (Moore, 1986). During BEACHON-ROCS, the separation was $\sim0.5$ m and wind speeds typically varied from 0.5 to 4.5 m s$^{-1}$, leading to errors ranging from 0.84% to 6.6%. Error resulting from dampening inside the inlet was predicted by the following cospectral transfer function:

$$T_s(f) = e^{-\frac{(2\pi f)^2 \Lambda L a}{u^2}} \tag{S4}$$

where $f$ is the cospectral frequency, $\Lambda$ is the attenuation coefficient, $L$ is the length of tubing, $a$ is the radius of the tubing inner diameter, and $u$ is the flow rate through the inlet (Massman, 1991). Dampening was considered for both the main inlet line ($\Lambda = 1$, $u = 18.7$ m s$^{-1}$, $L = 38.5$ m) and the internal instrument tubing ($\Lambda = 20$, u = 3.5 m s$^{-1}$, L = 1 m), resulting in a total error of 1.3%. Error resulting from the lag time calculation was calculated using the error in the fitted linear trends. Fluxes were calculated for the lag time range of the $1\sigma$ error in the trends, then the standard deviation over these fluxes were taken to be the lag contribution to the error. Median daytime error due to lag time was $\sim20\%$.

**S3  HCHO Production via CH$_3$O$_2$ Radical**

PA concentrations were calculated with a steady-state model, based on observations in a similar coniferous forest, which predicts the PA steady state concentration ($[PA]_{ss}$) by the steady-state equation:

$$[PA]_{SS} = \frac{P_{MVK} + P_{MACR} + P_{CH_3CHO} + P_{MGLY} + P_{BACE} + P_{PAN}}{L_{NO_2} + L_{NO} + L_{HO2} + L_{RO_2}} \tag{S5}$$

However, this equation simplifies significantly upon neglect of isoprene oxidation products, as isoprene has been observed to be low at this site (Kim et al., 2010):

$$[PA]_{SS} = \frac{k_{acetal \cdot OH}[CH_3CHO][OH] + k_d[PAN]}{k_{PA \cdot NO_2}[NO_2] + k_{PA \cdot NO}[NO] + k_{PA \cdot HO_2}[HO_2] + k_{PA \cdot RO_2}[RO_2]} \tag{S6}$$

Reactions of PA radical with NO and $RO_2$ have a unity yield of methylperoxy radical (CH$_3$O$_2$) (Atkinson et al., 2006), while reaction with $HO_2$ has a 40% yield through methyl hydrogen peroxide (Hasson et al., 2004; Jenkin et al., 2007; Dillon and Crowley, 2008). CH$_3$O$_2$ has a net unity yield of HCHO via reactions with NO, $RO_2$ (Tyndall et al., 2001; Atkinson et al., 2006), and $HO_2$ (Fried et al., 1997), which permits us to assume all CH$_3$O$_2$ radicals quickly react to form HCHO. This leads to a production rate of HCHO from PA radicals of:

$$P_{HCHO}^{PA} = P_{CH_3O_2}^{PA} = [PA]_{SS} \cdot (k_{PA \cdot NO}[NO] + k_{PA \cdot RO_2}[RO_2] + 0.4 \cdot k_{PA \cdot HO_2}[HO_2]) \tag{S7}$$

Similarly, OH-initiated oxidation of methane produces $CH_3O_2$ radicals (and thus HCHO) with unity yield. Methane concentrations were assumed to be constant at $1.7\ ppm_v$.

## S4 Aerodynamic and Laminar Sublayer Resistance

$R_a$ is the aerodynamic resistance, the resistance to transfer between the measurement height and the surface (Monteith, 1965).

$$R_a = \frac{\bar{u}(z-d)}{u_*^2} - \frac{\Psi_H(\xi) - \Psi_M(\xi)}{k \cdot u_*} \tag{S8}$$

where $z$ is measurement height A.G.L., $d$ is the displacement height ($2/3 \times h$), $\bar{u}(x)$ is the wind speed at height $x$, $k$ is the von Karman constant ($\sim$0.4), and $\Psi_H$ and $\Psi_M$ are the sensible heat and momentum integrated stability corrections (Dyer, 1974), which are a function of the stability parameter $x_i = (z-d)/L$, where $L$ is the Obukhov length. Typical values of $R_a$ range from $8\ s\ m^{-1}$ at mid-day to $30\ s\ m^{-1}$ at night. $R_b$ is the laminar sublayer resistance, the resistance to molecular diffusive transport through the viscous layer surrounding leaf surfaces (Jensen and Hummelshoj, 1995, 1997).

$$R_b = \frac{\nu}{u_* \cdot D_{HCHO}} \cdot \left[ \frac{100 \cdot l \cdot u_*}{LAI^2 \cdot \nu} \right]^{1/3} \tag{S9}$$

$\nu$ is the pressure-corrected kinematic viscosity of air ($1.7 \times 10^{-5}\ m^2\ s^{-1}$), $D_{HCHO}$ is the pressure-corrected diffusion coefficient for HCHO ($1.7 \times 10^{-5}\ m^2\ s^{-1}$) (Wesely, 1989; Massman, 1998), and $l$ is the "characteristic length scale", or thickness, of a pine needle (1 mm). Typical values of $R_b$ range from $16\ s\ m^{-1}$ at mid-day to $32\ s\ m^{-1}$ at night.

# References

Atkinson, R. and Arey, J.: Gas-phase tropospheric chemistry of biogenic volatile organic compounds: a review, Atmospheric Environment, 37, S197–S219, doi:10.1016/S1352-2310(03)00391-1, 2003.

Atkinson, R., Baulch, D. L., Cox, R. A., Crowley, J. N., Hampson, R. F., Hynes, R. G., Jenkin, M. E., Rossi, M. J., and Troe, J.: Evaluated kinetic and photochemical data for atmospheric chemistry: Volume II - gas phase reactions of organic species, Atmospheric Chemistry and Physics, 6, 3625–4055, 2006.

Carrasco, N., Doussin, J. F., O'Connor, M., Wenger, J. C., Picquet-Varrault, B., Durand-Jolibois, R., and Carlier, P.: Simulation chamber studies of the atmospheric oxidation of 2-methyl-3-buten-2-ol: Reaction with hydroxyl radicals and ozone under a variety of conditions, Journal of Atmospheric Chemistry, 56, 33–55, doi:10.1007/s10874-006-9041-y, 2007.

Dillon, T. J. and Crowley, J. N.: Direct detection of OH formation in the reactions of $HO_2$ with $CH_3C(O)O_2$ and other substituted peroxy radicals, Atmospheric Chemistry and Physics, 8, 4877–4889, 2008.

Dyer, A.: A Review of Flux-Profile Relationships, Boundary-Layer Meteorology, 7, 363–372, 1974.

Fried, A., McKeen, S., Sewell, S., Harder, J., Henry, B., Goldan, P., Kuster, W., Williams, E., Baumann, K., Shetter, R., and Cantrell, C.: Photochemistry of formaldehyde during the 1993 Tropospheric OH Photochemistry Experiment, Journal of Geophysical Research-Atmospheres, 102, 6283–6296, 1997.

Griffith, D. W. T.: Synthetic calibration and quantitative analysis of gas-phase FT-IR spectra, Applied Spectroscopy, 50, 59–70, 1996.

Hasson, A. S., Tyndall, G. S., and Orlando, J. J.: A product yield study of the reaction of $HO_2$ radicals with ethyl peroxy ($C_2H_5O_2$), acetyl peroxy ($CH_3C(O)O_2$), and acetonyl peroxy ($CH_3C(O)CH_2O_2$) radicals, Journal of Physical Chemistry A, 108, 5979–5989, doi:10.1021/Jp048873t, 2004.

Horst, T. W.: A simple formula for attenuation of eddy fluxes measured with first-order-response scalar sensors, Boundary-Layer Meteorology, 82, 219–233, 1997.

Hottle, J. R., Huisman, A. J., Digangi, J. P., Kammrath, A., Galloway, M. M., Coens, K. L., and Keutsch, F. N.: A Laser Induced Fluorescence-Based Instrument for In-Situ Measurements of Atmospheric Formaldehyde, Environmental Science & Technology, 43, 790–795, doi:10.1021/Es801621f, 2009.

Jenkin, M. E., Hurley, M. D., and Wallington, T. J.: Investigation of the radical product channel of the $CH_3C(O)O_2 + HO_2$ reaction in the gas phase, Physical Chemistry Chemical Physics, 9, 3149–3162, doi:10.1039/B702757e, 2007.

Jensen, N. O. and Hummelshoj, P.: Derivation of Canopy Resistance for Water-Vapor Fluxes over a Spruce Forest, Using a New Technique for the Viscous Sublayer Resistance, Agricultural and Forest Meteorology, 73, 339–352, 1995.

Jensen, N. O. and Hummelshoj, P.: Erratum to "Derivation of canopy resistance for water vapor fluxes over a spruce forest, using a new technique for the viscous sublayer resistance", Agricultural and Forest Meteorology, 85, 289–289, 1997.

Kim, S., Karl, T., Guenther, A., Tyndall, G., Orlando, J., Harley, P., Rasmussen, R., and Apel, E.: Emissions and ambient distributions of Biogenic Volatile Organic Compounds (BVOC) in a ponderosa pine ecosystem: interpretation of PTR-MS mass spectra, Atmospheric Chemistry and Physics, 10, 1759–1771, 2010.

Lee, A., Goldstein, A. H., Kroll, J. H., Ng, N. L., Varutbangkul, V., Flagan, R. C., and Seinfeld, J. H.: Gas-phase products and secondary aerosol yields from the photooxidation of 16 different terpenes, Journal of

Geophysical Research-Atmospheres, 111, doi:10.1029/2006jd007050, 2006.

Lenschow, D. H. and Kristensen, L.: Sampling Errors in Flux Measurements of Slowly Depositing Pollutants, Journal of Climate and Applied Meteorology, 25, 1785–1787, 1986.

Massman, W. J.: The Attenuation of Concentration Fluctuations in Turbulent-Flow through a Tube, Journal of Geophysical Research-Atmospheres, 96, 15 269–15 273, 1991.

Massman, W. J.: A review of the molecular diffusivities of $H_2O$, $CO_2$, $CH_4$, CO, $O_3$, $SO_2$, $NH_3$, $N_2O$, $NO_3$ and $NO_2$ in air, $O_2$ and $N_2$ near STP, Atmospheric Environment, 32, 1111–1127, 1998.

McManus, J. B., Zahniser, M. S., Nelson, D. D., Shorter, J. H., Herndon, S., Wood, E., and Wehr, R.: Application of quantum cascade lasers to high-precision atmospheric trace gas measurements, Optical Engineering, 49, Artn 111 124, doi:10.1117/1.3498782, 2010.

Monteith, J.: Evaporation and Environment, Symposia of the Society for Experimental Biology, 19, 205–234, 1965.

Moore, C. J.: Frequency-Response Corrections for Eddy-Correlation Systems, Boundary-Layer Meteorology, 37, 17–35, 1986.

Ritter, J. A., Lenschow, D. H., Barrick, J. D. W., Gregory, G. L., Sachse, G. W., Hill, G. F., and Woerner, M. A.: Airborne Flux Measurements and Budget Estimates of Trace Species over the Amazon Basin during the GTE/ABLE 2B Expedition, Journal of Geophysical Research-Atmospheres, 95, 16 875–16 886, 1990.

Rothman, L. S., Jacquemart, D., Barbe, A., Benner, D. C., Birk, M., Brown, L. R., Carleer, M. R., Chackerian, C., Chance, K., Coudert, L. H., Dana, V., Devi, V. M., Flaud, J. M., Gamache, R. R., Goldman, A., Hartmann, J. M., Jucks, K. W., Maki, A. G., Mandin, J. Y., Massie, S. T., Orphal, J., Perrin, A., Rinsland, C. P., Smith, M. A. H., Tennyson, J., Tolchenov, R. N., Toth, R. A., Vander Auwera, J., Varanasi, P., and Wagner, G.: The HITRAN 2004 molecular spectroscopic database, Journal of Quantitative Spectroscopy & Radiative Transfer, 96, 139–204, doi:10.1016/j.jqsrt.2004.10.008, 2005.

Tyndall, G. S., Cox, R. A., Granier, C., Lesclaux, R., Moortgat, G. K., Pilling, M. J., Ravishankara, A. R., and Wallington, T. J.: Atmospheric chemistry of small organic peroxy radicals, Journal of Geophysical Research-Atmospheres, 106, 12 157–12 182, 2001.

Weibring, P., Richter, D., Walega, J. G., and Fried, A.: First demonstration of a high performance difference frequency spectrometer on airborne, Optics Express, 15, 13 476–13 495, 2007.

Wesely, M. L.: Parameterization of Surface Resistances to Gaseous Dry Deposition in Regional-Scale Numerical-Models, Atmospheric Environment, 23, 1293–1304, 1989.

Wisthaler, A., Apel, E. C., Bossmeyer, J., Hansel, A., Junkermann, W., Koppmann, R., Meier, R., Muller, K., Solomon, S. J., Steinbrecher, R., Tillmann, R., and Brauers, T.: Technical Note: Intercomparison of formaldehyde measurements at the atmosphere simulation chamber SAPHIR, Atmospheric Chemistry and Physics, 8, 2189–2200, 2008.
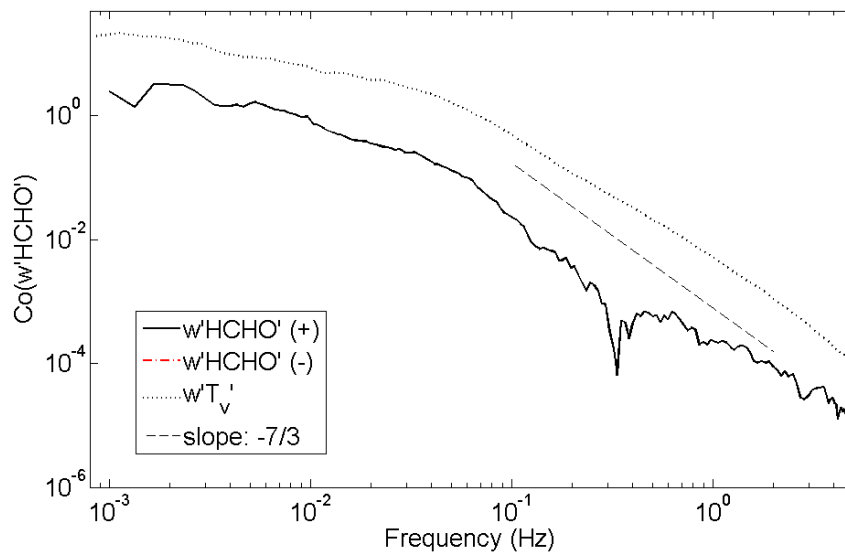
**Fig. S1.** Average cospectra of HCHO and virtual temperature with vertical wind speed during half-hour periods from 10 AM to 2 PM over entire measurement period. To compensate for noise, cospectra were binned into 200 bins spaced equally in frequency, and each bin was averaged. The red dot-dashed region in w'HCHO' denotes negative contributions to flux. The positive w'HCHO' points designate a positive covariance, whereas negative w'HCHO' points designate negative covariance .
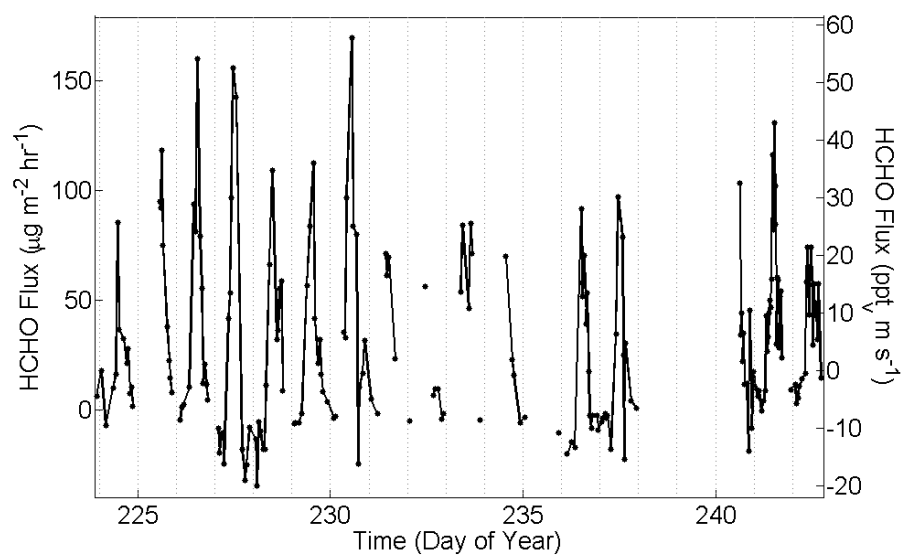
**Fig. S2.** Time series of HCHO flux over entire flux measurement period (11 - 30 August). Data has been corrected for unstationary conditions.
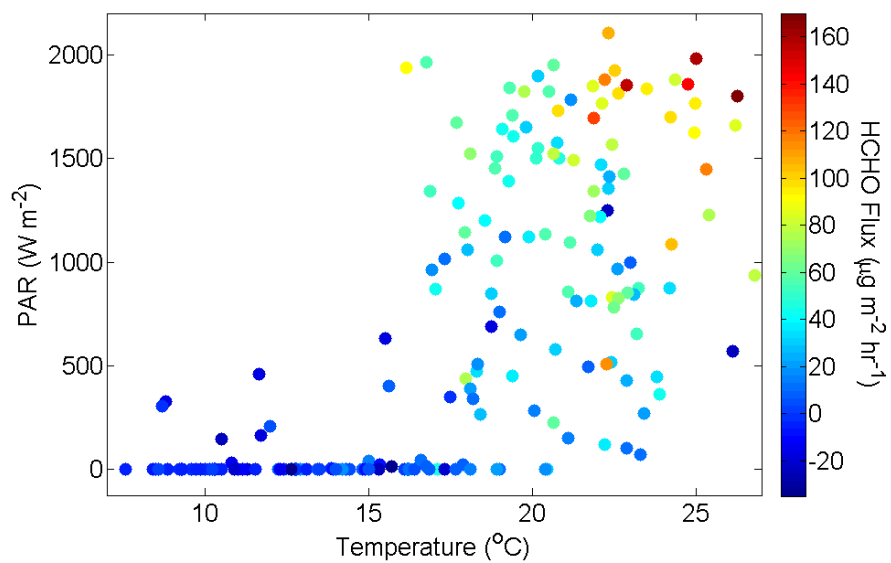
**Fig. S3.** Temperature and PAR dependence of HCHO flux during BEACHON-ROCS.

**Table S1.** Comparison of detection limits and time resolution of HCHO measurement techniques.

| Technique | $3\sigma$ Detection Limit | Reference |
|---|---|---|
| Quantum Cascade Laser Spectroscopy | $\sim$96 ppt$_v$ in 1 s | McManus et al. (2010) |
| Tunable Diode Laser Spectroscopy | $\sim$180 ppt$_v$ in 1 s | Weibring et al. (2007) |
| Proton Transfer Reaction-Mass Spectrometry | 300 ppt$_v$ in 2 s | Wisthaler et al. (2008) |
| Hantzsch Derivitization | 75 ppt$_v$ in 1 min | Wisthaler et al. (2008) |
| Madison Ti:Sapphire LIF | $\sim$51 ppt$_v$ in 1 s | Hottle et al. (2009) |
| Madison FILIF (field) | $\sim$300 ppt$_v$ in 1 s | this work |
| Madison FILIF (laboratory) | $\sim$25 ppt$_v$ in 1 s | this work |

**Table S2.** Chemical production and loss rates and yields for zero-dimensional box model. All rate constants have units of $\mathrm{cm^3 molec^{-1} s^{-1}}$ unless otherwise specified.

| Reaction | HCHO Yield | Yield Reference | Rate Constant T = temperature (K) | Rate Constant Reference |
|---|---|---|---|---|
| MBO + OH | 0.33 | a | $8.2 \times 10^{-12} \times e^{610/T}$ | d |
| $\alpha-$pinene + OH | 0.19 | b | $1.2 \times 10^{-11} \times e^{440/T}$ | d |
| $\beta-$pinene + OH | 0.51 | c | $7.89 \times 10^{-11}$ | b |
| Methanol + OH | 1.0 | d | $2.85 \times 10^{-12} \times e^{-345/T}$ | d |
| $3-$carene + OH | 0.28 | c | $8.68 \times 10^{-11}$ | b |
| Acetaldehyde + OH | 1.0 | d | $4.4 \times 10^{-12} \times e^{365/T}$ | d |
| $CH_4$ + OH | 1.0 | d | $1.85 \times 10^{-12} \times e^{-1690/T}$ | d |
| PAN $\rightarrow$ PA + $NO_2$ | - | - | $(*)\ k_0 : 4.9 \times 10^{-3} \times e^{-12100/T}$ $(*)\ k_\infty : 5.43 \times 10^{16} \times e^{-13830/T}$ $(**)\ F_c : 0.31$ | d |
| PA + $NO_2$ | - | - | $(*)\ k_0 : 2.7 \times 10^{-28} \times (T/300)^{7.1}$ $(*)\ k_\infty : 1.2 \times 10^{-11} \times (T/300)^{0.9}$ $(**)\ F_c : 0.31$ | d |
| PA + NO | 1.0 | d | $7.5 \times 10^{-12} \times e^{290/T}$ | d |
| PA + $HO_2$ | $\sim 0.4$ | e,f,g | $5.2 \times 10^{-13} \times e^{980/T}$ | d |
| PA + $RO_2$ | 1.0 | d | $2.0 \times 10^{-12} \times e^{500/T}$ | d |
| MBO + $O_3$ | 0.5 | a | $1.0 \times 10^{-17}$ | d |
| $\alpha-$pinene + $O_3$ | 0.28 | c | $6.3 \times 10^{-16} \times e^{-580/T}$ | d |
| $\beta-$pinene + $O_3$ | 0.65 | c | $1.5 \times 10^{-17}$ | b |
| $3-$carene + $O_3$ | 0.25 | c | $3.61 \times 10^{-17}$ | b |
| HCHO + OH | - | - | $5.4 \times 10^{-12} \times e^{135/T}$ | d |

a. Carrasco et al. (2007)

b. Atkinson and Arey (2003)

c. Lee et al. (2006)

d. Atkinson et al. (2006)

e. Hasson et al. (2004)

f. Jenkin et al. (2007)

g. Dillon and Crowley (2008)

\* Units: $s^{-1}$

\*\* Unitless

**Table S3.** Noon model case results in µg m$^{-2}$ hr$^{-1}$ by species.

| Species | Base | VOC-I | E350 | VOC-II |
|---|---|---|---|---|
| *Production:* | | | | |
| Litter Emission | 8.43 (25%) | 8.43 (7%) | 8.43 (6%) | 8.43 (15%) |
| MBO + OH | 8.35 (24%) | 83.5 (74%) | 8.35 (6%) | 8.35 (14%) |
| PPine Emission | 4.24 (12%) | 4.24 (4%) | 105 (78%) | 4.24 (7%) |
| PA | 3.99 (12%) | 3.99 (4%) | 3.99 (3%) | 3.99 (7%) |
| $CH_4$ + OH | 2.76 (8%) | 2.76 (2%) | 2.76 (2%) | 2.76 (5%) |
| $CH_3CHO$ + OH | 2.10 (6%) | 2.10 (2%) | 2.10 (2%) | 2.10 (3%) |
| $CH_3OH$ + OH | 1.16 (3%) | 1.16 (1%) | 1.16 (1%) | 1.16 (2%) |
| $\beta-$pinene + OH | 0.67 (2%) | 0.67 (1%) | 0.67 (<1%) | 6.69 (12%) |
| $\alpha-$pinene + OH | 0.61 (2%) | 0.61 (1%) | 0.61 (<1%) | 6.11 (11%) |
| Other MT + OH | 0.49 (1%) | 0.49 (<1%) | 0.49 (<1%) | 4.93 (9%) |
| MBO + $O_3$ | 0.48 (1%) | 4.80 (4%) | 0.48 (<1%) | 0.48 (1%) |
| $3-$carene + OH | 0.33 (1%) | 0.33 (<1%) | 0.33 (<1%) | 3.26 (6%) |
| Other MT + $O_3$ | 0.32 (1%) | 0.32 (<1%) | 0.32 (<1%) | 3.17 (6%) |
| $\alpha-$pinene + OH | 0.14 (<1%) | 0.14 (<1%) | 0.14 (<1%) | 1.41 (2%) |
| $\beta-$pinene + $O_3$ | 0.04 (<1%) | 0.04 (<1%) | 0.04 (<1%) | 0.40 (1%) |
| $3-$carene + $O_3$ | 0.03 (<1%) | 0.03 (<1%) | 0.03 (<1%) | 0.30 (1%) |
| *Loss:* | | | | |
| Dry Deposition | -19.30 (69%) | -22.37 (72%) | -27.19 (76%) | -19.30 (69%) |
| Photolysis | -4.90 (17%) | -4.90 (16%) | -4.90 (14%) | -4.90 (17%) |
| OH | -3.84 (14%) | -3.84 (12%) | -3.84 (11%) | -3.84 (14%) |